Validation of the performance of a practical blood vessel imaging system to facilitate vessel punctures

Cuper, Natascha, Verdaasdonk, Rudolf, de Roode, Rowland

Natascha J. Cuper, Rudolf M. Verdaasdonk, Rowland de Roode, "Validation of the performance of a practical blood vessel imaging system to facilitate vessel punctures," Proc. SPIE 7169, Advanced Biomedical and Clinical Diagnostic Systems VII, 716918 (24 February 2009); doi: 10.1117/12.809561

SPIE.

Event: SPIE BiOS, 2009, San Jose, California, United States

Validation of the performance of a practical blood vessel imaging system to facilitate vessel punctures

Natascha J. Cuper, Rudolf M. Verdaasdonk and Rowland de Roode,
Dept. of Medical Technology and Clinical Physics

University Medical Centre Utrecht, PO Box 85500, 3508 GA, Utrecht, The Netherlands
Correspondence: n.j.cuper@umcutrecht.nl

ABSTRACT

A practical system to visualize vessels underneath the skin has been developed, based on near-infrared (NIR) transillumination. A study in the clinical setting proved the system to be useful as a support in blood withdrawal in young children. During clinical application it was found that performance varied depending on vessel size, depth of vessels and surrounding lighting conditions. To gain more insight on the different variables that determine functioning of the system, we performed phantom studies. A combined liquid/solid phantom was fabricated with similar optical properties as the tissue layers of skin reported in literature at 850 nm. This phantom was used to estimate the depth of visibility in the relation to vessel size and darkness of the skin. Vessel contrast was determined analytically from images and evaluated by 3 independent observers. The knowledge gained from these experiments will be helpful to improve the imaging system and develop a solid phantom to be used as a gold standard to test the system under various clinical lighting conditions. The working range of the system was found to be appropriate to visualize the vessels used for the most procedures, such as blood withdrawal and placement of intravenous lines.

Keywords: near-infrared; vessel imaging; venipuncture; tissue phantom; optical properties

1. INTRODUCTION

An innovative vessel imaging system was developed by our department of Medical Technology and Clinical Physics. This system is able to visualize blood vessels underneath the skin by means of near-infrared light. A LED emitting infrared light with a wavelength of 850 nm is pressed at the opposite side of the puncture site. The light travels through the skin and is well absorbed by the blood vessels. A camera, sensitive to infrared light, captures a real-time image of the vessels. Figure 1 shows a schematic view of the system. Figure 2 shows a picture of a hand with blood vessels.

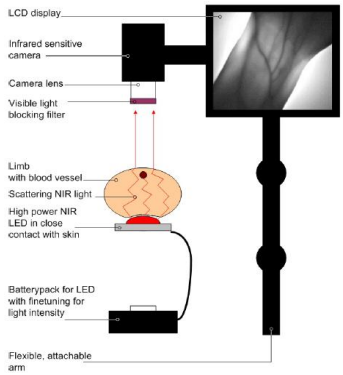

Figure 1. Schematic view of the vessel viewing system.

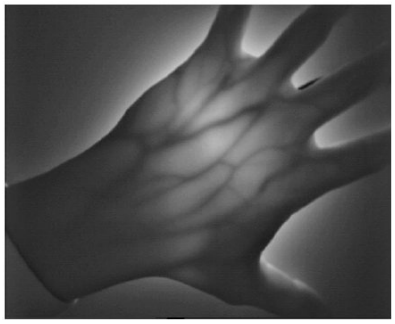

Figure 2. Image of a hand with blood vessels.

In a previous study[1], efficiency of the vessel viewing system in facilitating vessel puncture for blood withdrawal was proven. Failure rate (percentage of procedures were more than one puncture was necessary to gain blood) dropped from 13% to 2% for blood withdrawal procedures in children of 0 to 6 years of age. The technicians were very satisfied with the use of the system.

Advanced Biomedical and Clinical Diagnostic Systems VII, edited by Anita Mahadevan-Jansen, Tuan Vo-Dinh, Warren S. Grundfest, Proc. of SPIE Vol. 7169, 716918

The vessel imaging system is found to be well able to visualize most relevant vessels. However, although the concept of vessel viewing is not new, there is not much known in literature on parameters such as depth of visualization, influence of vessel diameter (blood filling) and influence of ambient light. Therefore a phantom was developed to measure visibility of vessels, related to diameter and depth. Also the influence of different amounts of pigment in the skin on visibility was measured. With the outcome of this study a solid phantom can be developed with vessels at various depths, that can be used to test different lighting conditions in clinical situations.

2. OPTICAL PROPERTIES OF SKIN

The layers of tissue located above the blood vessels are respectively the epidermis, the dermis and the subcutis embedding the blood vessels. Most of the blood vessels of importance for vessel puncture are on top of the musculature. Each of these layers contain chromophores influencing the absorption of light. In the epidermis, with an average thickness of 0.1 mm thick[2,3] , the main chromophore is melanin, a pigment that defines an individual's skin color. The dermis with an average thickness of 2 mm[2,3], has blood as its dominant chromophore. The blood vessels are situated in the subcutis. Figure 3 shows a schematic overview of the skin layers.

To construct a phantom of the optical properties of the skin, the absorption coefficient μ_a and the effective scattering coefficient $\mu_s(1\text{-}g)$ (or $\mu_s`$) need to be simulated for each of these layers. In literature, the data on optical properties of skin tissue shows a large variation due to the variance of absorption and scattering of tissue among individuals, as well as different ways to perform measurements. The optical properties chosen for our phantom are indicative for a 'standard' individual to be used to estimate the depth of visibility of blood vessels and the influence of skin color. In table 1, the optical properties of skin layers are presented as found or derived from literature.

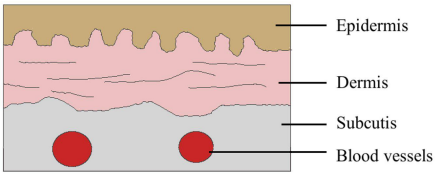

Figure 3. Tissue layers

	μ_a [cm^{-1}]	μ_s [cm^{-1}]	thickness (mm)
epidermis light	2	18,8/ 11.9/ 14.3±1.5	0.1
epidermis tanned	15	'	'
epidermis dark	29	'	'
epidermis very dark	50	'	'
dermis	0.26/ 0.33±.03	18,8/ 11.9/ 9.0±0.2	2
subcutis	0.09±.03 to 0.12±.04/ 0.06	12.1±3.2 to 10.8±2.7/ 11	various
arteries	4.98	31.5±1.2	various
veins	5.57	'	various

Table 1. Optical properties of tissue layers.

Epidermis

The absorption coefficient varies with the amount of melanin in the skin, and thus with skin color. Four skin types with different volume fractions (f_v) of melanosomes are used in our phantom.

Those are: light-skinned (f_v 2%), tanned (f_v 13%), dark skinned (f_v 25%) and very dark (f_v 43%)[4]. The absorption coefficient of the epidermis of the different skin types is determinded according a paper by Jacques [4] at $\lambda = 850$ nm.

The scattering coefficient of skin (epidermis and dermis) was derived based on calculations by Bashkatov et al [5] and is $\mu_{s\ skin}` = 18.8$ cm$^{-1}$ at $\lambda = 850$ nm. Other authors like Cheong et al[6] reported scattering coefficients of $\mu_{s\ epi}` = 14.3 \pm 1.5$ cm^{-1} for pig epidermis and $\mu_{s\ derm}` = 9.0 \pm 0.2$ for pig dermis.

Dermis

The main chromophore in the dermis is blood. The amount of blood is heterogeneously distributed in the dermis, due to local plexi of vessels. Assuming a homogenous distribution of blood with 0.2 % as the volume fraction of blood in the dermis[4] , the ratio between arterial and venous blood 50/50 with a mean oxygen saturation of 80%, the absorption coefficient for blood can be derived: $\mu_{a\ blood} = 5{,}27$ cm^{-1} s and $\mu_{a\ derm} = 0.26$ cm^{-1}. The figure reported by Cheong et al [6] is $\mu_{a\ derm} = 0.33 \pm 0.03$ cm^{-1} for pig dermis. The scattering coefficient can be assumed to be comparable with the epidermis.

Subcutis
The subcutis between the dermis and the bloodvessels consists mainly of fat cells. Simpson et al[8] reported $\mu_{a\ sc}$` to be 0.09±0.03 cm^{-1} at 700 nm and 0.12±0.04 cm^{-1} at 900 nm. Cheong et al. did not report on subcutis, however, present a figure for adipose tissue in the pig of $\mu_{a\ derm} = 0.06\ cm^{-1}$ at 789 nm. Scattering coefficient for fatty tissue was calculated using Bashkatov et al [5], $\mu_{s\ sc}` = 11\ cm^{-1}$ at 850 nm. In comparison, Simpson et al[8] found $\mu_{s\ sc}`$ 12.1±3.2 cm^{-1} at 700 nm and 10.8±2.7 cm^{-1} at 900 nm.

Blood vessels
The main chromophore in blood is hemoglobin. The absorption coefficient of blood can be calculated using :
$\mu_{a\ blood} = (f_{v\ hbo2} * \mu_{a\ hbo2}) + (1 - f_{v\ hbo2}) * \mu_{a\ hb}$ [cm^{-1}]
With $f_v = 0.65$ for venous blood and $f_v = 0.95$ for arterial blood, the absorption coefficient for a vein is $\mu_{a\ blood\ venous} = 4.98\ cm^{-1}$ and the absorption coefficient for a artery is $\mu_{a\ bloodarterial} = 5.57\ cm^{-1}$
Scattering is ascribed to the red blood cells and reported by Lovell et al [9] to be $\mu_{s\ blood}` = 31.5 \pm 1.2\ cm^{-1}$

3. COMPOSITION OF TISSUE PHANTOM

3.1. Substrate

As substrate for the solid phantom layers epoxy resin (Polypox THV 500, Poly-service, The Netherlands) was used to dissolve the pigments and scatter particles. Epoxy resin is optically clear at 850 nm and has been used in solid phantoms [10,11] before. For the liquid layer, water was used.

3.2. Absorbers

Various pigments were applied as absorbers. Indian ink was well soluble in water while phtalocyanin powder (Lukas pigments, Genuine Green) and natural sepia powder, containing melanin [12] were mixed with epoxy.
Each pigment was mixed at a series of increasing concentration in the substrate and measured with a spectrophotometer at 850 nm to determine the absorption in relation to concentration as presented in the graph of figure 4.
For each pigment, the mean ratio absorbance/ concentration is determined along with the standard deviation. For sepia the ratio is 1.1±0.1; for phtalocyanin the ratio is 1.4±0.3, for Indian ink the ratio is 29±3.

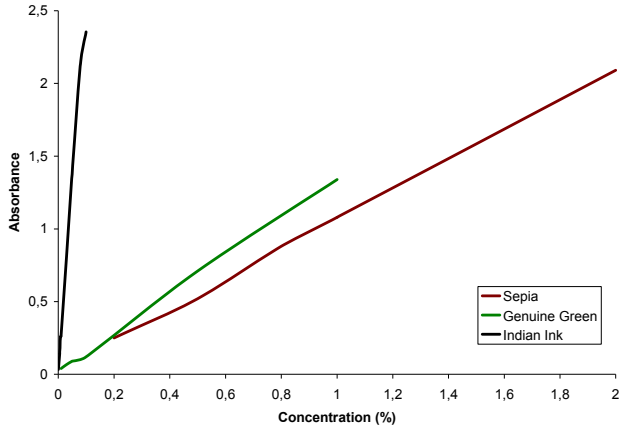

Figure 4. Absorbance of three different pigments, plotted to concentration, measured in a 1 cm cuvette.

3.3. Scatter materials

Intralipid is a solution of water and purified soybean oil, used for intravenous feeding and has been proven effective as scatter material in in tissue phantoms before[13]. The reduced scattering coefficient of 0.01% Intralipid at a specific wavelength can be derived [13] using $\mu_s(\lambda) = 0.016\,\lambda^{-2.4}$ and $g(\lambda) = 1.1 - 0.58\,\lambda$ (±5%)
Titaniumdioxide is used before as a scatter material in epoxy phantom[10,14]. The reduced scattering coefficient is approximately 9±1 cm^{-1} in a solution of 1 mg TiO_2 per milliliter epoxy resin.

3.4. Blood vessels

The blood vessels are made of epoxy mixed with 3.5 mg of TiO_2 p/ml epoxy resin and 1.6% phtalocyanin solution to obtain a μ_a of 5±1 cm^{-1} and a μ_s of 35±4 cm^{-1}. This mixture is injected with a syringe into urinary catheters as mould. After curing of the epoxy, the urinary catheter was removed from it. Four sizes of blood vessels were created: 1 mm, 1.6 mm, 2.6 mm and 3.6 mm.
For the skin layer, epidermis and dermis are combined in one layer which since the epidermis is only 0.01 cm thick. The absorption coefficients for the different skin types are shown in table 1. With the dermis being 2 mm thick and a $\mu_a = 0.3$ cm^{-1}, the combined absorption coefficient is respectively 0.04, 1.1, 1.8 and 2.8 cm^{-1}. Scattering coefficient μ_s was chosen to be 15 cm^{-1}. Epoxy resin is mixed with 1.7 mg/ml TiO_2 to obtain a μ_s of 15±2 cm^{-1}. A concentration of respectively 0.016%, 0.44%, 0.72% and 1.12% sepia solution is used to obtain a μ_a of 0.04±0.003 cm^{-1}, 1.1±0.1 cm^{-1}, 1.8±0.1 cm^{-1} and 2.8±0.2 cm^{-1}. The epoxy resin is cast into petri dishes of 13.5 cm diameter.

3.5. Construction of layered skin phantom

The tissue phantom was designed to enable the positioning of artificial blood vessels at various depths. Therefore, the top layer (epidermis and dermis) was made of a solid sheet while a liquid (intralipid) represents the subcutis in which artificial vessels are moved to specific depths.
The solid layer of the skin phantom is floating on top of the intralipid. The blood vessels are mounted on a frame which can be lowered stepwise in the intralipid bath. Figure 5 shows a schematic of the setup.

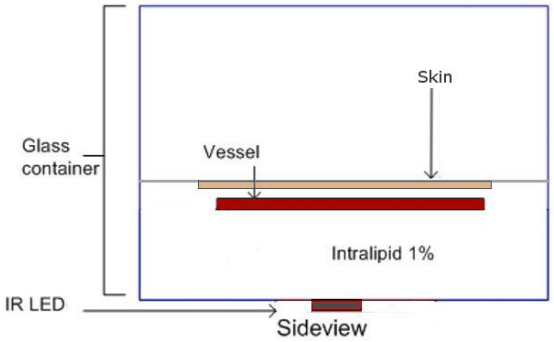

Figure 5. Schematic view of the experimental setup.

The intralipid bath acts as a phantom of the subcutis/fat layer where the blood vessels are situated. A concentration of 0.1% Intralipid is used, which gives a scattering of approximately 9 cm^{-1}. Indian Ink (0.0014%) is diluted into the Intralipid to obtain a μ_a of 0.10±0.01 cm. The bath is filled with 3 cm of Intralipid 1%.

	Materials	μ_a [cm^{-1}]	μ_s [cm^{-1}]
skin light	epoxy/ sepia (0.016%) / TiO_2 (1.5 mg/ml)	0.04	15
skin tanned	epoxy/ sepia (0.44%) / TiO_2 (1.5 mg/ml)	1.1	15
skin dark	epoxy/ sepia (0.72%) / TiO_2 (1.5 mg/ml)	1.8	15
skin very dark	epoxy/ sepia (1.12%) / TiO_2 (1.5 mg/ml)	2.8	15
Subcutis	water/ / ink (0.0014%)/ Intralipid (1%)	0.1	9
blood vessels	epoxy/ phtalocyanin (1.6%)/ TiO_2 (3.5 mg/ml)	5	35

Table 2. Materials used for the phantom and their optical properties.

4. METHODS

4.1. Depth of visibility

The frame with a blood vessel mounted on is put in the intralipid bath. Underneath the bottom of the optically clear tank a LED is placed, exactly as it would be in a patient when the vessel imaging system is used. The light intensity of the LED shows a Gaussian spreading. The vessel is positioned in the middle of the spot.
The vessel imaging system captures a movie of two seconds from the vessel, when it is just beneath the liquid surface. Then the vessels are lowered by steps of 0.3 mm for the smallest vessel and steps of 0.6 mm for the larger vessels. At every step, a video sequence is captured. As reference, the light spot without vessels is captured.
Several measurements are performed: firstly, an experiment with every diameter vessel in the intralipid bath without the skin phantom on top, following, experiments with the vessels of 1.6 mm and 3.6 mm diameter in the bath, with each skin type consecutively on top.

4.2. Analysis

The images were processed for quantification. To reduce noise, the 50 frames from each 2 second movie clip are combined into one bitmap. This way a bitmap per vessel for each consecutive step and a bitmap of the white reference is created. From each bitmap, 50 horizontal image lines from the middle of the intensity spot perpendicular on the vessel are combined and averaged into one scan line (see figure 6). An offset (lowest intensity value) is determined for each bitmap. Using the following formula, the relative value of the intensity decrease in relation to the white reference is determined:

$$\frac{MV - offset}{whiteref - offset} = RV$$

MV: measured value (scan line), RV: relative value

Per vessel a graph is made of the relative value per vertical pixel, per lowering step. Figure 7 shows the relative values per pixel, for four lowering steps (step 0, 1,2 and 5).. The noise in this part is in the order of magnitude of the third digit. Ideally, the graph, with exception of the location of the vessel should be aligned with value 1 at the y-axis after subtracting the white reference. However, the graph is asymmetrical. This is ascribed to the internal gain and a low accuracy of the video recording system.

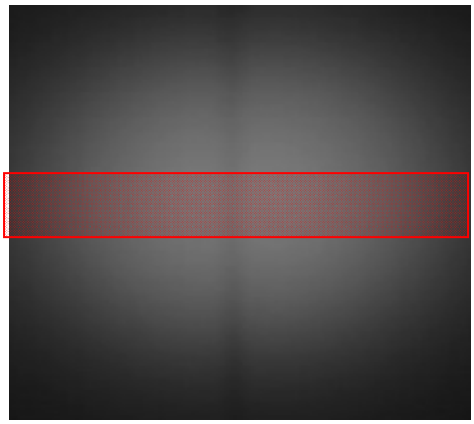

Figure 6. Bitmap of combined 50 frames showing a 1 mm vessel at a depth of 1 mm. The box shows the area of the 50 horizontal image line to determine the average scan line.

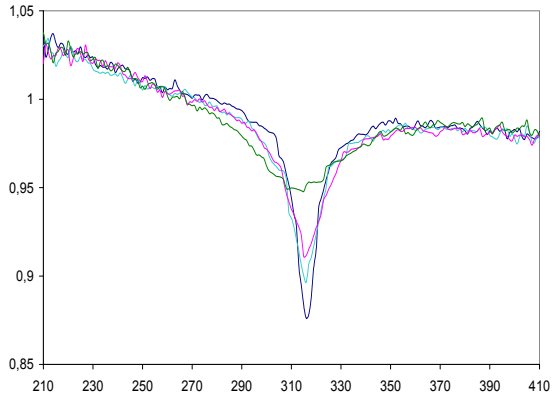

Figure 7. Relative values to image pixels of a vessel of 1 mm thickness, for four lowering steps (step 0, 1, 2 and 5).

To correct for the asymmetry, a quadratic polynomial plus gaussian function was fitted to the data as shown in figure 8. Using the polynoom the baseline for 100 % background intensity was determined and normalized to 1. From each sequence of increasing depth per vessel, ΔI was calculated (the difference between top and basis) as shown in figure 9.

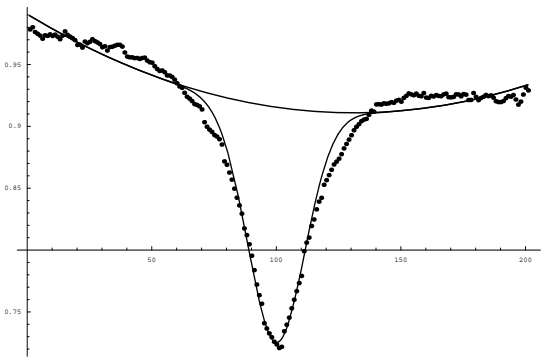

Figure 8. Polynoom and Gaussian fit on data

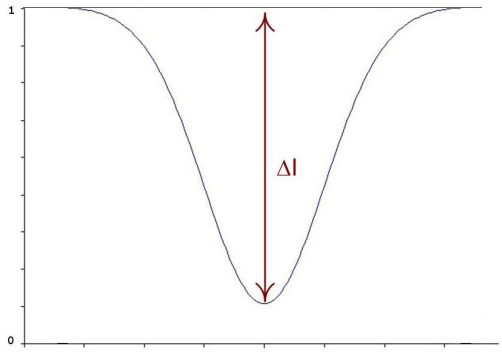

Figure 9. ΔI determined from intensity drop from in normalized data fit

4.3. Visibility to observers

Besides the quantification of the images, 3 independent observers were asked to judge to which depth they could distinguish the vessels from the background. This provided the link between the quantitative data measured and the visibility representative for the clinical setting.

5. RESULTS

In figure 10 the intensity drop for the 4 vessel diameters is presented in relation to the depth in the bath of 1 % Intralipid with μ_a=0.1 cm^{-1}. There is a gap between the two smaller and the two bigger vessels. This may be ascribed to light that is transmitted through the vessels themselves. The maximum depth of visibility in relation to the vessel size determined by three independent observers is presented in figure 11.

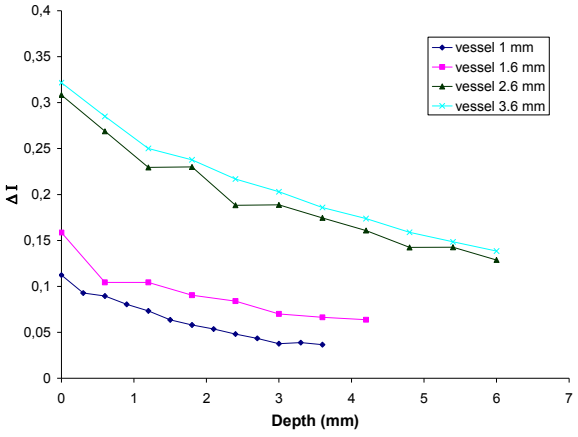

Figure 10. Relative intensity drop ΔI for various diameter vessel in relation to depth underneath the surface

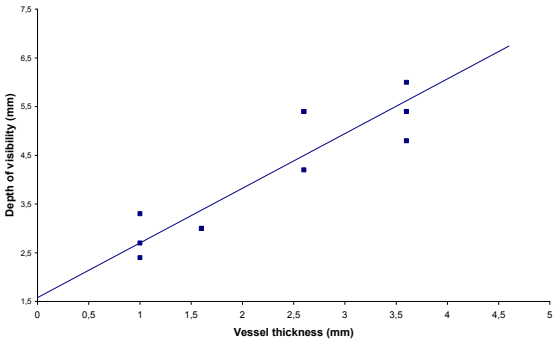

Figure 11. Maximum depth of visibility correlated to the vessel size in milimeters, dertermined by 3 observers

The results from figure 10 and 11 are combined in figure 12 to obtain a better insight between the quantitative data and the visibility to the human eye.

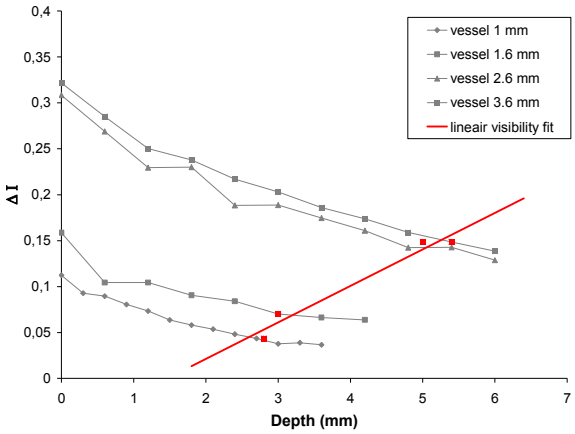

Figure 12. Combination of relative intensity drop (grey lines) and maximum depth of visibility of the vessels by observers (dots and lineair fit in red).

For the different skin types the results are presented in figure 13 and 14. The contrast ratio increases for a darker skin type. It was expected that intensity drop would not be dependent on tissue type since the scattering coefficient was dominant ($\mu_a << \mu_s$). The finding that the contrast increases with a darker skin type might be attributed to the auto gain of the camera system which adjusts itself when less overall light is received.

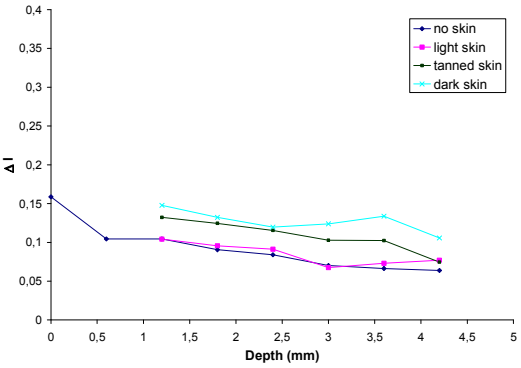

Figure 13. Relative intensity drop, Δ I, in relation to depth for a 1.6 mm diameter vessel for different skin types.

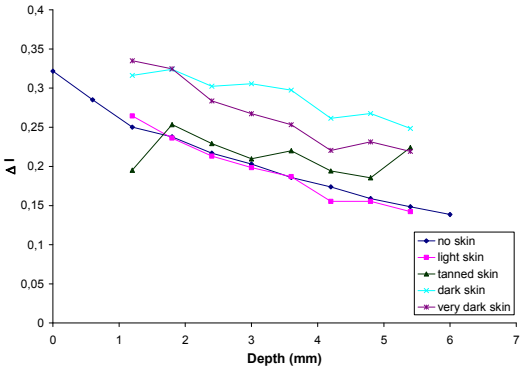

Figure 14. Relative intensity drop, Δ I, in relation to depth for a 3.6 mm diameter vessel for different skin types

6. DISCUSSION

In this study, we have attempted to quantify the visibility of a vessel in relation to diameter and depth in a tissue phantom. Combined with maximum depth of visibility determined by observers, it should possible to estimate the depth at which a particular diameter vessel can still be observed using our vessel imaging system (see figure 12). This provides a tool to test the performance and usability of the system.

The results from this study do not yet provide a reliable qualification method due to the following causes:

- quantification of images obtained with the video capture system has proven difficult due auto gain operations by the camera and recording hardware which influences the contrast of details in the images.
- It was not known if the camera has a linear response to a range of intensities in which the skin types were tested
- The Gaussian distribution of the light from the IR source under the tissue phantom showed variations and an asymmetric behaviour which had to be corrected for.

However, these limitations in the experimental setup are related to the use of the vessel viewing system as it is used in the clinic and would provide information how this clinical system performs.

In a following study, we could have a better control over the variables such as: camera hardware set to fixed gain and an uniform illumination underneath the tissue phantom. This would probably provide a better standard for testing the vessel viewing system in various conditions [15].
Based on the experience from this study a solid epoxy phantom with vessels can be developed. This phantom can be used as a "golden standard" to test the functionality of the vessel imaging system in different lighting conditions in the clinic. Experience using the vessel viewing system in clinical conditions have shown that the presence of strong infrared light in the environment e.g. daylight or light bulbs interfere with the visibility performance of the system. Using the tissue phantom, the conditions can be optimized e.g blocking daylight and turning off the OR lamp.
After the positive results from the first patient studies, we have started to develop a commercial version of our vessel imaging system that will become available during 2009 and is intended to be provide assistance during blood withdrawal and vessel puncture procedures throughout hospital in both children and adults.

7. CONCLUSION

The tissue phantom developed showed to be useful to test the performance of a vessel imaging system. It is possible to estimate up to which depth a vessel of a particular diameter can be observed . It was proven that the vessel imaging system is capable to visualize the most relevant vessels. As expected, the darkness of the skin is of minor influence for visualization of vessels.

REFERENCES

[1] Cuper, N. J., Verdaasdonk, R. M., Roode, R. d., and Septer, E. "Development and clinical trial of a practical vessel imaging system for vessel punctures in children", SPIE. **6848**, 684806. 2008. San Jose, CA, USA.
[2] Anderson, R. R. and Parrish, J. A., "The optics of human skin", J.Invest Dermatol.77, 13-19 (1981).
[3] Krishnaswamy, A. and Baranoski, G. V. G., "A biophysically-based spectral model of light interaction with human skin", C.G.F.23, 331-340 (2004).
[4] Jacques, S. L. "*http://omlc.ogi.edu/news/jan98/skinoptics.html*" . 1998. Oregon Medical Laser Center. 20-8-2007.
[5] Bashkatov, A. N., Genina, E. A., Kochubey, V. I., and Tuchin, V. V., "Optical properties of human skin, subcutaneous and mucous tissues in the wavelength range from 400 to 2000 nm", Journal of Physics D-Applied Physics38, 2543-2555 (2005).
[6] Cheong, W. F., Prahl, S. A., Welch, A. J., Wang, L., and Jacques, S. L. "*http://omlc.ogi.edu/pubs/pdf/cheong90a.pdf*" . 1990. Oregon Medical Laser Center.
[7] Prahl, S. A. "*http://omlc.ogi.edu/spectra/hemoglobin/index.html*" . 1999. Oregon Medical Laser Center. 15-1-2009.
[8] Simpson, C. R., Kohl, M., Essenpreis, M., and Cope, M., "Near-infrared optical properties of ex vivo human skin and subcutaneous tissues measured using the Monte Carlo inversion technique", Phys.Med.Biol.43, 2465-2478 (1998).
[9] Lovell, A. T., Hebden, J. C., Goldstone, J. C., and Cope, M. "Determination of the transport scattering coefficient of red blood cells", SPIE. **3597**, 175-182. 1999. Bellingham, WA, USA, Society of Photo-Optical Instrumentation Engineers.
[10] Firbank, M. and Delpy, D. T., "A design for a stable and reproducible phantom for use in near-infrared imaging and spectroscopy", Phys.Med.Biol.38, 847-853 (1993).
[11] Firbank, M., Oda, M., and Delpy, D. T., "An improved design for a stable and reproducible phantom material for use in near-infrared spectroscopy and imaging", Phys.Med.Biol.40, 955-961 (1995).
[12] Urso, P., Lualdi, M., Colombo, A., Carrara, M., Tomatis, S., and Marchesini, R., "Skin and cutaneous melanocytic lesion simulation in biomedical optics with multilayered phantoms", Phys.Med.Biol.52, 229-239 (2007).
[13] Staveren, H. J., Moes, C. J. M., Marle, J., Prahl, S. A., and Gemert, M. J. C. v., "Light scattering in Intralipid-10% in the wavelength range of 400-1100 nm", Appl.Opt.30, 4507-4514 (1991).
[14] Hebden, J. C., Price, B. D., Gibson, A. P., and Royle, G., "A soft deformable tissue-equivalent phantom for diffuse optical tomography", Phys.Med.Biol.51, 5581-5590 (2006).
[15] Sharp, R., Adams, J., Machiraju, R., Lee, R., and Crane, R., "Physics-based subsurface visualization of human tissue", Ieee Transactions on Visualization and Computer Graphics13, 620-629 (2007).